This is the peer reviewed version of the following article: Naseer, M. R., Li, L., Zou, J., Leung, R. C. K., Liu, Y., & Maryami, R. (2024). Experimental Study of Deep Cavity Noise Suppression by Surface Compliance. In 30th AIAA/CEAS Aeroacoustics Conference (2024). American Institute of Aeronautics and Astronautics, which has been published in final form at https://doi.org/doi:10.2514/6.2024-3280.

Experimental Study of Deep Cavity Noise Suppression by Surface Compliance

Muhammad Rehan Naseer[1,a], Lin Li[2,b], Jiaju Zou[3,b],
Randolph C. K. Leung[4,a], Yu Liu[5,b] and Reza Maryami[6,b]

[a] *Department of Mechanical Engineering, The Hong Kong Polytechnic University, Kowloon, Hong Kong, People's Republic of China*

[b] *Department of Mechanics and Aerospace Engineering, Southern University of Science and Technology, Shenzhen, Guangdong 518055, People's Republic of China*

This study investigates a novel passive control technique for suppressing tonal noise in deep cavities, focusing on the strategic use of surface compliance. An experimental setup was designed, featuring a deep cavity with an elastic panel flush-mounted at the cavity bottom. The primary goal is to verify and extend the findings of the previous numerical study by Naseer, et al. [1], which explored the potential of leveraging aeroacoustic-structural interactions for noise suppression. Pressure measurements of cavity flow and farfield noise, along with Particle Image Velocimetry (PIV), were utilized to capture the interactions between flow dynamics and the cavity acoustic response. The experimental results demonstrated that the panel effectively altered the aeroacoustic pattern inside the cavity, leading to a noticeable reduction in tonal noise up to 16.1 dB, particularly at specific flow velocities, 20 and 30 ms^{-1}, where the interaction between shear layer oscillations and cavity acoustic modes typically strengthens aeroacoustic resonance. The study provides a detailed analysis of the modified aeroacoustic feedback mechanisms due to the introduction of the elastic panel. A comparison of acoustic spectra between the baseline rigid cavity configuration and the modified cavity-panel setup revealed that the panel not only reduced the peak noise levels but also shifted the dominant acoustic frequencies, suggesting a disruption in the typical aeroacoustic coupling processes. These findings highlight the potential of using compliant surfaces to passively control aeroacoustic emissions in practical applications, offering a promising alternative to more invasive noise mitigation strategies.

I. Introduction

Cavity noise reduction is a compelling area of aeroacoustic research due to its significance in various mechanical systems. Under certain conditions, airflow can induce self-sustained oscillations that couple with acoustic modes, resulting in intense noise. These oscillations present substantial challenges across a range of engineering applications, from low-speed to high-speed environments. For example, in weapon bays and wheel wells, fluctuation in density and pressure invokes extreme noise and vibrations, particularly during the deployment of stores in military aircraft [2, 3]. Similar noise problems occur in railways with escalating noise from train car and bogie gaps as speeds increase [4, 5],

---

[1] PhD Candidate, Department of Mechanical Engineering.

[2] PhD Candidate, Department of Mechanics and Aerospace Engineering.

[3] Undergraduate Assistant, Department of Mechanics and Aerospace Engineering.

[4] Associate Professor, Department of Mechanical Engineering, Senior Member AIAA.

[5] Associate Professor, Department of Mechanics and Aerospace Engineering, AIAA Associate Fellow.

[6] Senior Research Fellow, Department of Mechanics and Aerospace Engineering.

and in the automotive industry with disruptive sunroof buffeting [6]. Gas transportation also faces issues with aeroacoustic pulsations leading to potential mechanical failures [7-9], while turbomachinery struggles with noise from unsteady shear layers [10, 11]. The intricacies involved in the cavity flow application therefore highlight the earnest need for innovative and sustainable solutions in mitigating cavity aeroacoustics.

Open cavity flow exhibits strong tonal noise at discrete frequencies, with a subtle difference between shallow ($L/D > 1$) and deep ($L/D < 1$) cavities. Covert [12] first observed these differences, with further refinement by Heller and Bliss [13] who noted distinct aeroacoustic coupling patterns in deep cavities, where the depthwise cavity acoustic mode was believed to interact with the shear layer oscillation. Rockwell and Naudascher [14] classified these behaviours as types of fluid-resonant oscillations driven by acoustic reinforcement of shear layer instabilities at the cavity leading edge due to either transverse or longitudinal acoustic modes. Rossiter [15]developed a theoretical model for these oscillations, particularly for shallow cavities, providing an empirical formula to predict their frequencies. This model highlights a feedback loop initiated by Kelvin-Helmholtz instabilities in the shear layer, whose interactions at the cavity trailing edge propagate upstream to sustain oscillations. The Rossiter model effectiveness has been validated and expanded in further studies [16, 17], confirming its applicability across various conditions.

Extensive research studies [9, 18, 19] show that oscillations at the opening of deep cavities activate internal acoustic modes, leading to significant noise radiation. These cavities differ from shallow ones, yet an adjusted Rossiter formula effectively predicts oscillation frequencies [13]. Particularly, when flow frequencies closely align with the cavity natural modes, deep cavities achieve maximal acoustic resonance [18, 19], highlighting the complex interplay between flow dynamics and acoustic responses. Bruggeman, et al. [7] proposed an alternative feedback mechanism rooted in vortex sound theory [20], involving resonant acoustic excitation of the shear layer, vortex formation from instabilities, and energy transfer to the acoustic field. This interaction can destabilize the shear layer and enhance vortex coalescence, explaining the lock-on effect often observed in deep cavities [19, 21, 22], thus deepening our understanding of fluid-resonant oscillations in cavity flows. Naseer, et al. [1] detailed the aeroacoustic feedback in deep cavities, identifying five key processes (as shown in Figure 3(b)): the development of a boundary layer at the upstream wall, emanation and evolution of the shear layer from the leading edge, impingement of developed vortices at the trailing edge, convection of vortices over the downstream wall, and the generation and reflection of pressure waves that close the feedback loop.

Recent years have seen the development of various passive (such as Figure 1(a)) and active techniques to modify cavity flow dynamics, targeting Rossiter modes to reduce noise [23-27]. Notably, Maury, et al. [28] used micro-perforated panels to decrease cavity pressure fluctuations by up to 8 dB, maintaining fundamental flow characteristics. [29] replaced flow jets with plasma actuators at the leading edge, achieving significant noise reduction with optimized actuation energy. Further, Bacci and Saddington [30] explored the effects of structural modifications, such as gaps at cavity edges, which improved aeroacoustic responses and modified fluid-acoustic interactions. Also, their Hilbert–Huang spectral analysis on cavities Bacci and Saddington [31] with fluidic spoilers showed that these devices could effectively reduce acoustic noise and alter shear layer trajectories. However, these techniques are flow-invasive and may introduce disturbances that alter the cavity original flow properties, potentially causing unintended aerodynamic consequences like increased turbulence or drag, and requiring higher energy inputs, issues still underexplored in literature.

This experimental study primarily aims to verify a unique concept of cavity noise suppression that has been previously explored numerically by Naseer, et al. [1], involving the use of surface compliance, provided by an elastic panel strategically positioned across critical locations on the cavity walls. The core principle hinges on exploiting the aeroacoustic structural interaction (Figure 1(b)), where an elastic panel mounted at the cavity bottom wall is excited by the incident cavity acoustic mode, thereby dissipating its energy into panel vibrations. This interaction is expected to disrupt the aeroacoustic processes within the cavity, thereby influencing the overall noise emissions. Moreover, the study also seeks to experimentally investigate the mechanism of cavity noise reduction through the decoupling of the cavity shear layer and acoustic mode using the described method. A key aspect of this approach is its non-invasive nature, contrasting with traditional methods; it aims to maintain the overall characteristic features of cavity flow while subtly and intuitively altering the interaction between the shear layer and the cavity acoustic mode. Therefore, a detailed exploration of the shear layer dynamics and cavity acoustic mode has also been performed. Lastly, the study will experimentally ascertain the ultimate noise reduction potential of this scheme, which could inform its transition to practical implementation in real-world engineering applications, as we have provided an elaborative design strategy for our novel cavity-panel configuration.

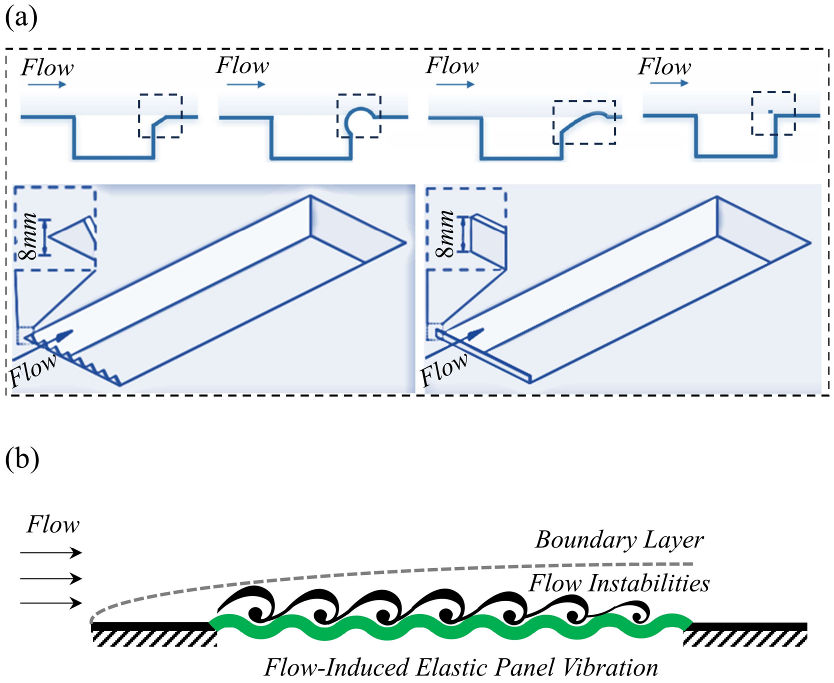

Fig. 1 (a) Traditional cavity noise reduction techniques (reproduced from Liu and Gómez [26], Saddington, et al. [32] with the permission of the authors). (b) The novel cavity noise suppression concept proposed in Naseer, et al. [1].

II. Experimental Setup

A. Aeroacoustic Wind Tunnel

The experimental study is carried out in a low-velocity, closed-circuit, open-jet wind tunnel at the Department of Mechanics and Aerospace Engineering, Southern University of Science and Technology (SUSTech) [33] as illustrated in Figure 2. The test section of the wind tunnel, which corresponds to the nozzle exit, features a rectangular cross-section with dimensions of 600 mm × 550 mm. The wind tunnel is capable of achieving flow velocity up to 70 ms^{-1} within the test section, with an accompanying turbulence intensity of 0.15% in the incoming nozzle flow. The wind tunnel resides inside an anechoic chamber with internal dimensions of 3.8 m × 5.7 m × 3 m (Figure 2(a)). To ensure a quasi-two-dimensional flow across the cavity model, a pair of rectangular endplates, each 800 mm in length, are aligned with the nozzle exit. The cavity model is vertically positioned between these plates (Figure 2(b), situated 270 mm downstream from the nozzle exit. Consequently, the model is effectively located within the potential core of the nozzle jet flow. The wind tunnel acoustic background noise at 25 ms^{-1} is 20 dB (relative to 20 µPa reference pressure), measured 1m from the center of the jet at 1m vertical height outside the main flow. The study is carried out with nozzle flow velocities ranging from 10 to 40 ms^{-1} with 5 ms^{-1} increments.

B. Cavity Flow Measurements

Characteristic flow pressure measurements are carried out by employing two pressure taps shown as *mic*2 and *mic*3 in Figure 2(c), strategically positioned along the cavity median. The first pressure tap is located near the cavity trailing edge at (x, y) = (30 mm, -7.5 mm) while the second pressure tap is located near the cavity bottom at (30 mm, -67.5 mm), as delineated in Figure 3(a). The pressure tap *mic*2 is located in the shear layer impingement region to capture the unsteady shear layer signatures of the certain flow and tested rigid cavity/panel configurations. Similarly, *mic*3 is located near the cavity bottom region to capture the acoustic signature of the cavity depthwise mode across the cases. Such a choice of microphone locations is informed by our previous study [1]. Each pressure tap featured a Panasonic WM-61A microphone with a 2 mm effective diaphragm diameter. The Panasonic WM-61A microphones, renowned for their extensive application in previous research [34-36], were selected for their proven fidelity in capturing pressure fluctuations within the 20 Hz to 10 kHz frequency range.

C. Cavity Noise Measurement

Acoustic signals in the far field were quantified utilizing a Brüel & Kjær Type 4966 free-field microphone (depicted as *mic*1 in the discussion ahead) placed orthogonal to the airflow at a standoff distance of 400 mm from the central axis of the cavity, as depicted in Figure 2(c). Data acquisition for both aeroacoustic flow pressure and far-field acoustic emissions was performed concurrently by employing a National Instruments PXI-10420 chassis equipped with a pair of synchronized 24-bit NI PXI-4496 data acquisition cards, operating at a sampling rate of 51.2 kHz across a duration of 20 seconds. For spectral analysis, the time-series pressure data were transformed into the frequency domain utilizing a Fast Fourier Transform (FFT) algorithm with a Hamming window function and 50% overlap, adhering to Welch method, thus achieving a frequency resolution of 2 Hz. Subsequently, the obtained spectra were processed to yield power spectral density (*PSD*) estimates, denoted with the unit dB/Hz for flow pressure and far-field acoustic fluctuations.

D. PIV Setup

Cavity acoustic phenomena sprouts from the shear layer evolution and trailing edge impingement, identified as the primary locus of noise generation, is investigated through a high-speed planar Particle Image Velocimetry (PIV) system. The scrutinized measurement domain, encompassing an approximate area of 40 mm × 30 mm, spanned across the area between the cavity leading and trailing edges where the aeroacoustic regime dominates the flow. This region is delineated by the rectangular green illuminated zone presented in Figure 2(c) and Figure 2(d). PIV experiments were conducted for both cavity configurations (*RC* and *EP*) and free-stream velocities 20 and 30 ms^{-1}. The flow was populated with dioctyl sebacate particles, with a mean diameter of 1µm, to serve as tracer particles. A Photonics Nd:YAG laser, delivering 45 mJ pulses at a repetition rate of 1000 Hz, was strategically placed outside the flow field. Light-sheet optics were utilized downstream of the airfoil to illuminate the tracer particles.

Flow field imaging was accomplished using a Phantom VEO410L camera (resolution: 1,280 × 780 pixels, 12-bit, pixel pitch: 20 µm) paired with a Nikon 100 mm lens at an f/4 aperture setting. The camera was positioned approximately 500 mm from the measurement area at mid-span, which yielded an optical magnification of around 0.2. The LaVision DAVIS 10.0 software suite, in conjunction with a LaVision Programmable Time Unit, facilitated the synchronization of laser pulsing and camera triggering, as well as the image acquisition. The PIV system operated at a sampling frequency of 2.56 kHz, capturing images over a 5-second interval, which resulted in a comprehensive collection of 5,120 double-frame images. The comprehensive dataset, comprising 5,289 images, was subjected to processing through an iterative multipass algorithm, culminating in a final interrogation window dimension of 32 × 32 pixels, with an overlap factor set at 75%. To mitigate the influence of specular reflections from the surface during the PIV procedure, the surface of the cavity-embedded base structure received a matte black coating. Moreover, careful adjustment of the laser illumination incidence angle was performed to optimize the visualization of the seeded flow. This precise alignment of the laser angle was pivotal in reducing the quantity of light directly reflected into the camera sensor, thereby substantially enhancing the quality of the resultant images for PIV evaluation.

E. Design of Cavity Model and Elastic Panel

An open cavity with length L = 30 mm, depth D = 75 mm and vertical span W = 550 mm is taken. It is prepared in the form of a cutout from a model base structure 530 mm long and 100 mm thick (Figure 2(c) and 2(d)). Its span is 550 mm which gives a perfect fitting between the two endplates for ensuring two dimensionality of flow around the cavity. The choice of the length-to-depth ratio (L/D = 0.4) is the same as in the numerical study of Naseer, et al. [1]. In the present study, a coordinate system is set with its origin positioned at the center point of the leading edge of the cavity. The x-, y- and z-axes are set along the streamwise direction, cavity depth and cavity model span respectively.

The cavity-embedded base structure consists of a 150 mm long super-elliptic nose section following the recommended specifications to avoid flow separation [37]. The downstream side of the super-elliptic nose section is connected to a 230 mm long parallel section of 100 mm thickness and a 150 mm long tapered tail section with a 30° apex angle. The trailing edge geometry is inspired by Moreau, et al. [38] work as they showed that the sharp-edged flat plate tends to produce broadband noise. Therefore, it was helpful to have a distinguishable cavity tonal noise largely unaffected by the base model noise. A modular experimental rig was manufactured to accommodate both the rigid cavity, identified as *RC*, baseline case (Figure 3(a)) as well as the cavity-panel configuration, defined as *EP* in Figure 3(c), to verify the aeroacoustic suppression effect. The cavity modular design is actually based on five different parts, the upstream super-elliptic nose, the sharply tapered downstream plate and the former and latter are fixated together by a bottom plate and two small transparent plates are punched across the base structure to expose the cavity cutout section for the PIV instrumentation. For the *RC* case, a rigid plate of dimension 130 mm × 25 mm × 550 mm is inserted at the cavity bottom.

The specific choice of the mounting location of the elastic panel at the cavity bottom was informed by Naseer, et al. [1]. Among the five distinct aeroacoustic processes (each supported by different cavity walls) as shown in Figure 3(b) using an elastic panel, two configurations EP_{aft} and EP_{bottom} distinguished themselves by significantly suppressing cavity noise. The case EP_{aft} aimed to pacify the shear layer impingement process at the cavity aft wall, while the case EP_{bottom} focused on mitigating the incident cavity acoustic mode. Comparable in performance, both the configurations showed high effectiveness in noise suppression up to 4.8 dB (Figure 3(b)). However, the relatively simpler design and easier implementation of the EP_{bottom} panel encouraged its selection for our experimental campaign.

In addition to the panel mounting location, a critical aspect of the panel design strategy is ensuring that the natural frequency of the elastic panel, under fluid loading, matches the dominant flow frequency of the targeted RC case and in the current scenario, the targeted frequency is 1585 Hz at a freestream velocity of 30 ms^{-1}, where the cavity generates its maximum acoustic response. To achieve the desired aeroacoustic-structural resonance condition, the fluid-loaded panel natural vibration frequency for the desired mode (n) with fixed-end boundary conditions is calculated using the formula $(f_{EP})_n = (n/2L_{EP})[(T_{EP}/\rho_{EP}h_{EP})/(1 + L_{EP}/\pi n\rho_{EP}h_{EP})]^{0.5}$. While maintaining the panel length L_{EP} equal to the cavity length, adjustments to the thickness h_{EP} and the applied tension T_{EP} are made to align the panel frequency with the design requirements. In this study, the panel is assumed to be made of an elastomeric material such as a silicone rubber sheet with a thickness of 0.2 mm, following the recommendations from our previous study (Naseer, et al. [39]). To configure the experimental setup for EP, the rigid bottom plate of RC was replaced by a similarly dimensioned elastic panel embedded into the bottom plate. This panel was stretched and secured over two circular rods, fitting snugly into grooves etched across the adjacent cavity plates. A 10 mm gap was maintained beneath the panel to accommodate expected vibrations. The panel backside was exposed to ambient pressure through a series of large-sized holes in the elastic panel bottom plate. Notably, these backside holes also facilitate the insertion of probes for measuring the panel vibration frequency and tension using the Sonic Tension Meter U-550 by Gates Unitta Asia. This design not only ensures effective aeroacoustic interaction but also facilitates the necessary dynamics of the panel.

(a) *Experimental Setup* (b) *Schematic of Cavity Flow Model Setup*

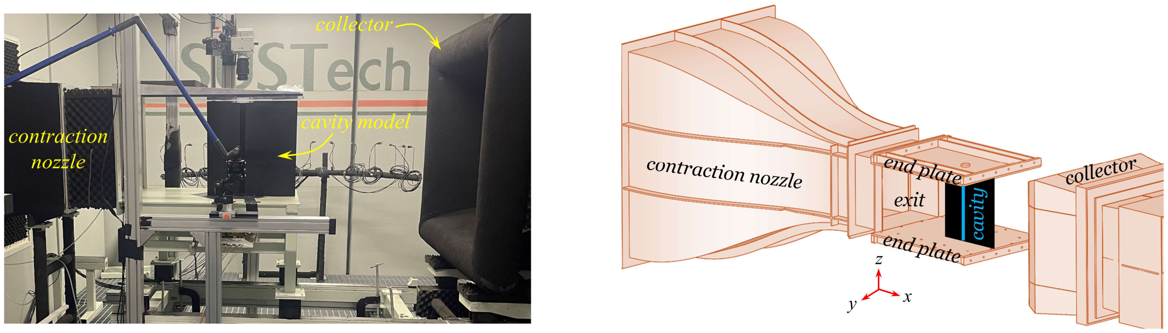

(c) *Top View* (d) *Front View*

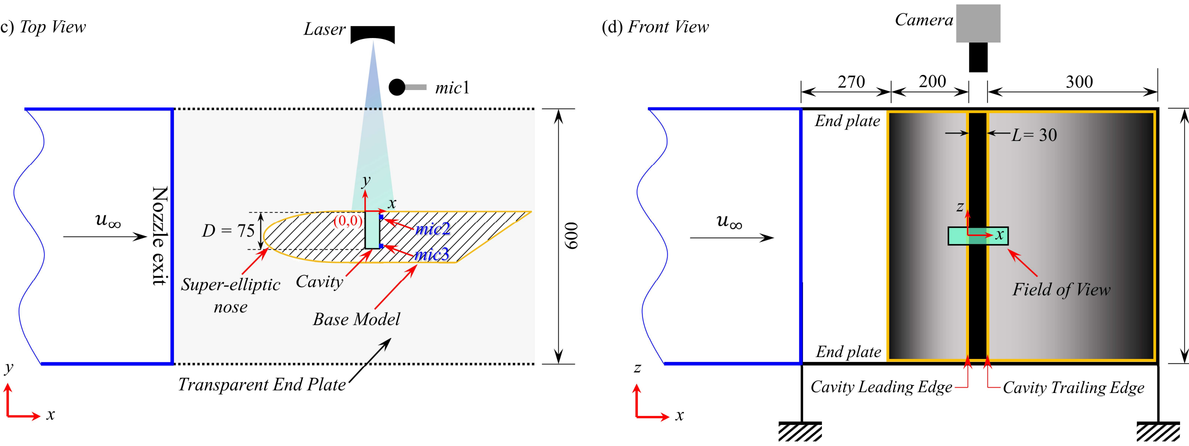

Fig. 2 (a) Experimental arrangements of open cavity flow, instrumented with surface and far-field microphones and PIV setup in the aeroacoustic wind tunnel (b) schematic diagram depicting the cavity flow model setup, (c) top view, (d) front view. Units for dimension: mm.

(a) *RC*

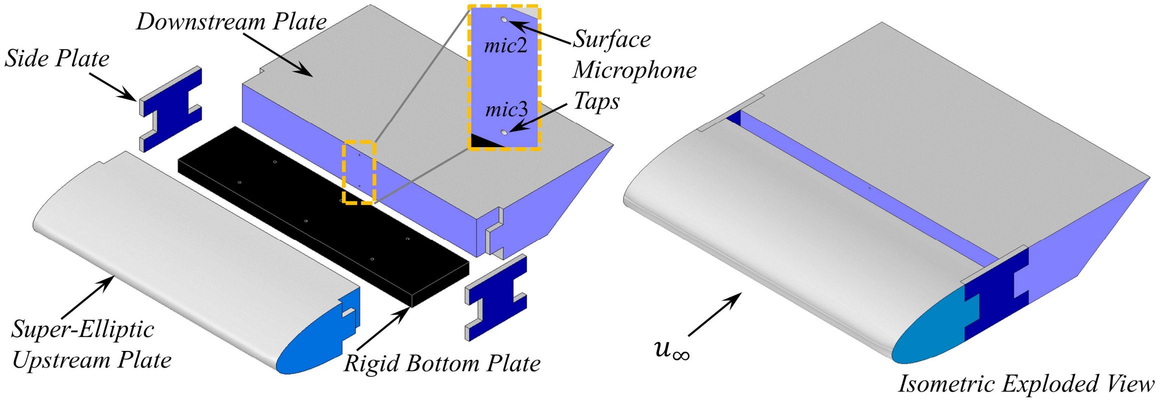

(b) Cavity aeroacoustic processes

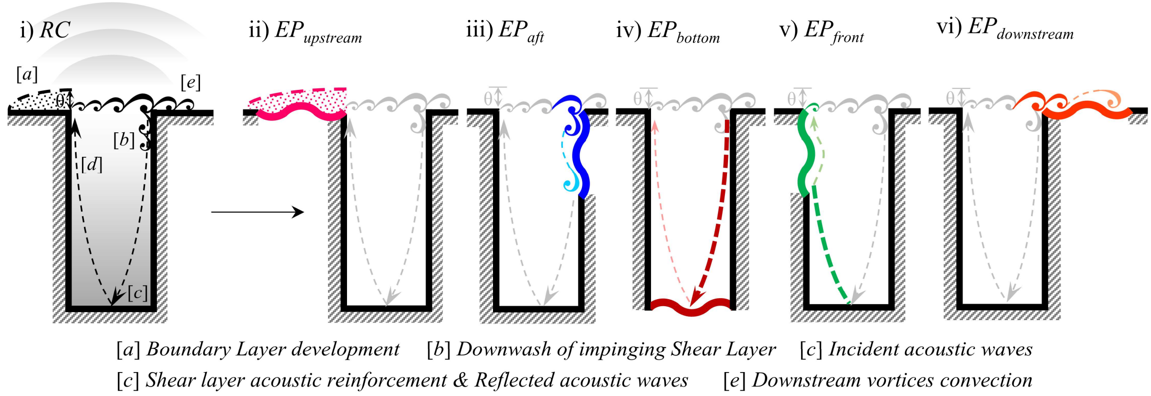

Cases	$EP_{upstream}$	EP_{aft}	EP_{bottom}	EP_{front}	$EP_{downstream}$
Sound Power Level, ΔPWL (dB)	– 1.3	– 4.8	– 4.6	– 1.1	+3.2

(c) *EP*

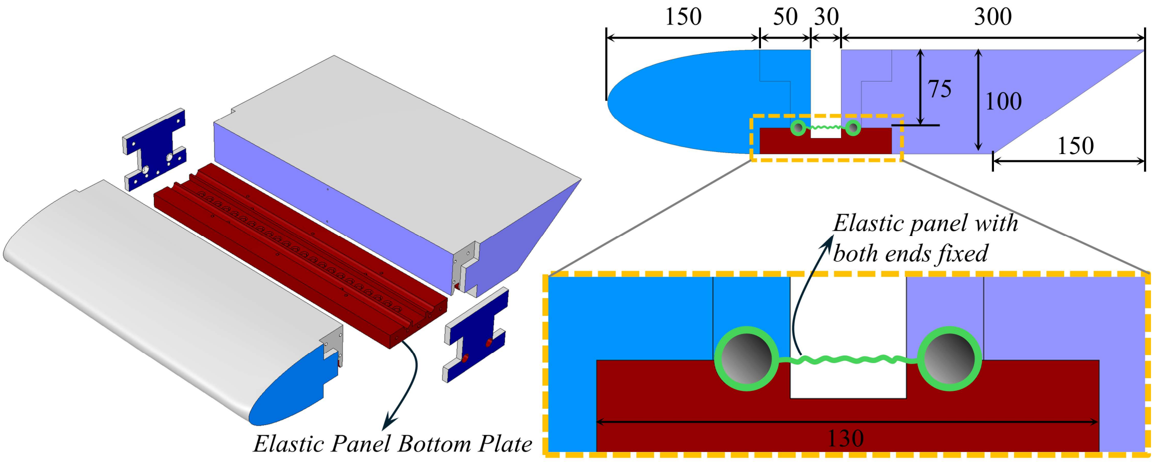

Fig. 3 Schematic of the physically informed cavity testing model design, (a) exploded views of *RC* modular design, (b) identified physical processes leading to cavity noise generation [1] and the corresponding elastic panel mounting locations for the noise suppression, (c) design of *EP* configuration. Units for dimension: mm.

III. Aeroacoustic characteristics

A. Rigid Cavity Noise Spectra

Figure 4 presents the power spectral density (*PSD*) of acoustic pressure for the *RC* cases, examined across seven free-stream flow velocities (u_∞ = 10, 15, 20, 25, 30, 35 and 40 ms^{-1}). PSD is calculated using PSD (dB/Hz) $= 10\log_{10}(p'/p_{ref})$, with reference pressure taken as p_{ref}= 20 µPa and p' is the pressure fluctuation. In order to ascertain the relative impact of base structure noise (absent the cavity feature), the cavity was filled and sealed to render a continuous, uninterrupted plane surface. The comparative analysis reveals that the model noise, with and without the cavity presence, is significantly disparate, exhibiting a difference of up to 40 dB across the relevant frequency range. Moreover, the background noise remains insignificant under all tested free-stream conditions. Given these conditions, the experimental setup offers a robust foundation for investigating cavity-generated noise.

The acoustic signature of the cavity noise features a pronounced tonal peak, indicative of the acoustic and aeroacoustic phenomena occurring inside the cavity confines. The increase in the fundamental frequency of this tonal noise is observed proportionally with the free-stream velocity. Additionally, the broadband noise contribution becomes more prominent across the entire frequency range and is amplified with increasing free-stream velocities. These findings align with the results from prior cavity flow research conducted by [22, 40], which identified that the peak acoustic response of the cavity occurs at u_∞ = 30 ms^{-1} due to strong aeroacoustic interaction between the shear layer and the cavity acoustic mode. This peak has been similarly identified in the present experiments, where noise radiation escalates with the free-stream velocity, reaching a tonal peak of 87.4 dB at u_∞= 30 ms^{-1} before reducing to 78.4 dB at u_∞ = 40 ms^{-1}. Instances exhibiting sharp tonal peaks emphasize the predominant influence of aeroacoustic mechanisms in driving the overall noise radiation. However, the coupling strength between the shear layer and acoustic modes varies amongst the cases, influencing the overall acoustic response of the cavity.

Table I presents a comparison of the peak frequencies obtained from the experimental cases with those calculated using the Heller and Bliss modified Rossiter formula, $f_{Heller\&Bliss}= (m-\alpha)/(\,1/\kappa + M_\infty/(1+(\gamma-1)M_\infty^2/2)^{0.5}\,)$, incorporating a universally chosen set of empirical constants [13]. The comparison reveals a generally good agreement between the experimentally measured Rossiter modes and those predicted by the formula. However, the Heller and Bliss formula tends to overestimate the Rossiter modes with the exception of the condition at a free-stream velocity of 30 ms^{-1}. Deviations between the experimental results and the computed frequencies are ascribed to the application of a uniform set of empirical constants across varying free-stream conditions, which, according to several studies [1, 29], should be custom-fitted for each specific scenario. Additionally, there is a noteworthy comparison between the peak frequencies observed in a previous numerical study of *RC* with a similar aspect ratio (*L/D* = 0.4) subjected to a free-stream velocity of u_∞= 30 ms^{-1} and its experimental counterpart, with a nominal discrepancy of merely 5%. This congruence further streamlined the numerical and experimental observations.

It is noteworthy that the *RC* noise spectrum for each flow velocity displays a number of tonal peaks corresponding to the Rossiter modes and their higher harmonics. At a freestream velocity of 10 ms^{-1}, there are five tonal peaks, while at 15 ms^{-1} and 20 ms^{-1}, there are three. As the freestream velocity increases, the number of peaks corresponding to the Rossiter modes or their higher harmonics decreases to two or fewer. For velocities of 35 ms^{-1} and 40 ms^{-1}, the prominence of tonal peaks diminishes, and the spectrum assumes a more broadband shape. In summary, the overall cavity flow appears to sustain the aeroacoustic feedback phenomenon, as evidenced by the persistent appearance of Rossiter modes across the range of operating conditions tested.

Table I Comparison of experimentally measured peak frequencies with the Heller formula.

u_∞ (ms^{-1})	m	α	M_∞	k	$f_{Heller\&Bliss}$ (Hz)	f_{Exp} (Hz)	$\Delta f = \lvert f_{H\&B} - f_{Exp}\rvert / f_{H\&B}$ (%)
10	2	0.25	0.03	0.57	327.1	340	3.9
15	2	0.25	0.045	0.57	486.5	485	0.3
20	3	0.25	0.06	0.57	1011.1	895	11.5
25	3	0.25	0.074	0.57	1253.7	1080	13.8
30	3	0.25	0.09	0.57	1492.5	1585	6.2
35	2	0.25	0.1	0.57	1099.3	1005	8.6
40	2	0.25	0.12	0.57	1246.5	1180	5.3

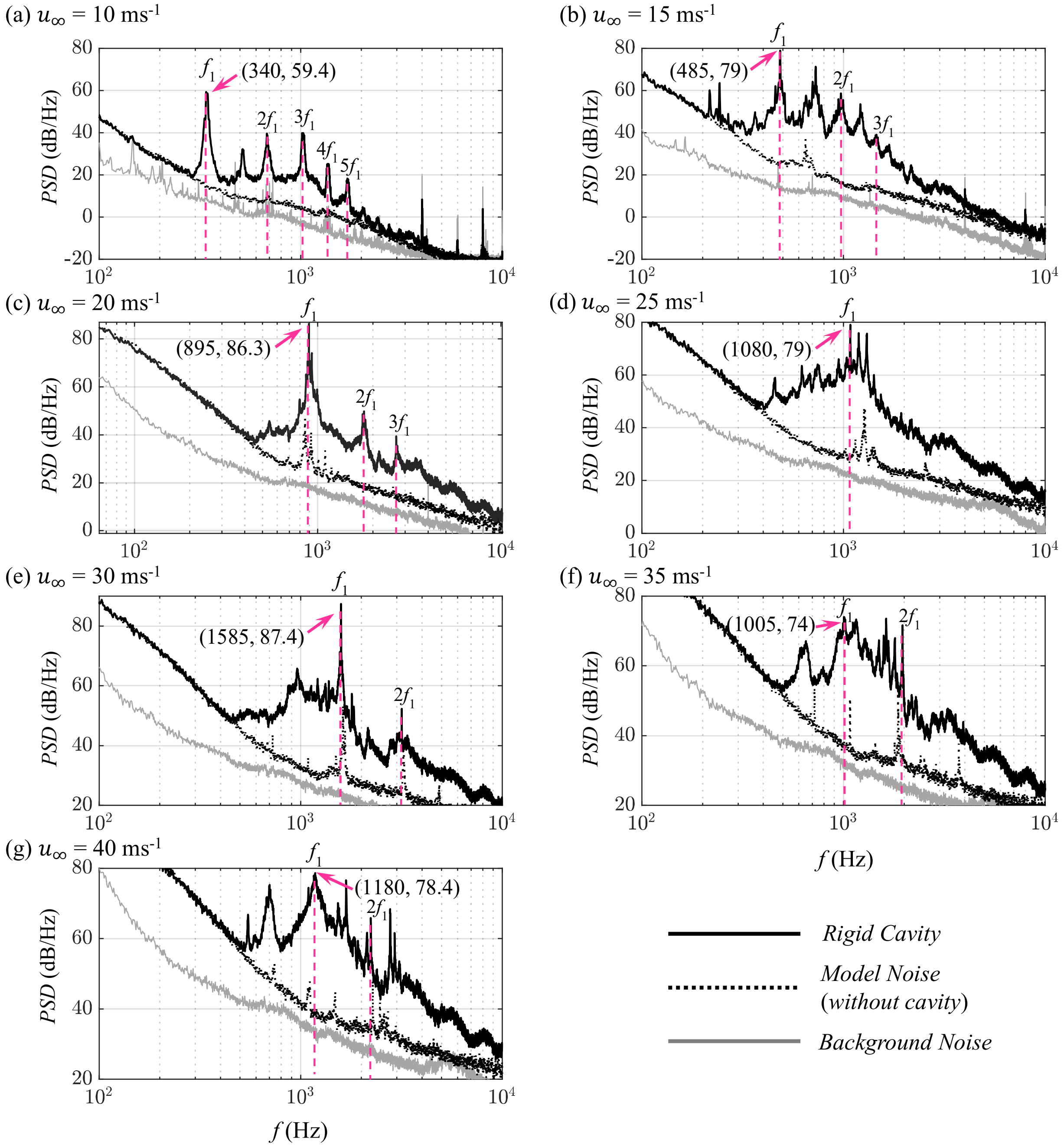

Fig. 4 Rigid Cavity noise measured at mic1 for various freestream flow conditions. The peak frequencies are labelled across each testing case.

B. Aeroacoustics of *RC* and *EP* Configurations

The aeroacoustic feedback mechanism, particularly how the coupling between the shear layer and cavity acoustic modes influences noise radiation in deep cavities, has been previously studied theoretically, numerically and experimentally [14, 19, 40-44]. Nevertheless, a rigorous experimental study of the corroboration of these aeroacoustic interactions and their precise effect on resultant noise radiation has not been fully elucidated. The primary question remains whether the influence is largely attributable to oscillations within the shear layer or to the acoustic resonant modes within the cavity depth. To elucidate the sequence of events—from the impingement of the shear layer on the cavity to the excitation of the cavity acoustic modes and their consequent interplay leading to noise radiation—a comparative analysis of pressure spectra at three strategically placed probe locations is employed. This comparison aims to dissect their frequency content and associated phenomena. In the following discussion, a total of four representative RC configurations are selected as baselines to gauge the efficacy of their RC counterparts in mitigating cavity noise.

To understand the mechanisms of noise generation and attenuation in both the RC and EP setups, the power spectral density (PSD) of pressure signals from the cavity flow and for acoustic fields were simultaneously measured. These measurements were taken using $mic2$ (to characterize the shear layer), $mic3$ (to capture the acoustic mode), and $mic1$ (to observe the far-field noise) and were analyzed in accordance with Heller and Bliss [13] modified Rossiter formula. Figure 5 illustrates the findings for selected RC /EP configurations under an array of free-stream flow conditions, specifically at velocities of u_∞= 10, 20, 30, and 40 ms^{-1}.

The power spectral density (PSD) spectra for the baseline RC conditions manifest a prominent tonal peak at the f_1-tone frequency, consistently observed across measurements of the shear layer, acoustic mode, and far-field noise, agreeing with the fundamental tone depicted in Tabel I. The surface pressure fluctuations captured at $mic2$ and $mic3$, sharing this peak frequency, are the potential contributors and the primary sources of acoustic radiation. For case $RC10$, the peak PSD of the shear layer exceeds that of the cavity acoustics, suggesting that the energy transfer from the shear layer impingement at the cavity trailing edge to the cavity acoustic mode is not effectively established. Conversely, in cases $RC20$ and $RC30$, the peak PSD of the cavity acoustics overtake that of the corresponding shear layer tone, indicating a proficient transfer of energy from the shear layer to the cavity acoustics, resulting in enhanced acoustic radiation. This enhancement implies the presence of an aeroacoustic feedback resonance mechanism. An additional observation across the far-field spectra for cases $RC10$, $RC20$, and $RC30$ is that they predominantly mimic the trends of their respective cavity acoustic mode spectra rather than those of the shear layer. Furthermore, the far-field tone remains proportionate with the cavity acoustic mode in $RC10$ or slightly exceeds it in cases $RC20$ and $RC30$. The $RC40$ case, however, exhibits a distinct pattern: the shear layer and cavity acoustic mode possess peak PSD tones of equal magnitude, which diverges from trends observed in prior cases. Moreover, the far-field spectral trends and levels do not align with those of the cavity acoustic mode in $RC40$, and the case lacks the sharply defined peaks evident in the other cases. Consequently, this suggests that the aeroacoustic resonance phenomenon diminishes as higher free-stream flow conditions are reached.

Figure 5 also presents a comparative analysis of the shear layer, cavity acoustics, and far-field noise spectra for the elastic panel configurations ($EP10$, $EP20$, $EP30$, and $EP40$), measured at the same probe locations as their RC counterparts. The spectral examination reveals that $EP20$ and $EP30$ exhibit peak tonal noise reductions of 9.2 dB and 16.1 dB, respectively, relative to their RC benchmarks ($RC20$ and $RC30$). In contrast, $EP10$ and $EP40$ configurations do not demonstrate any significant reduction, as their spectra remain largely unaltered. This suggests that the implementation of an elastic panel is effective in conditions ($RC20$ and $RC30$) where strong aeroacoustic interactions—between shear layer oscillations and cavity acoustic modes—are expected to drive fluid resonance within the cavity. However, the panel does not appear to have a discernible impact on other flow conditions ($RC10$ and $RC40$), where the cavity noise is presumed to be predominantly influenced by shear layer oscillations alone (fluid dynamic oscillation).

Apart from $EP30$, spectral analysis across the EP and RC cases displays a consistent tonal peak frequency pattern in the shear layer, cavity acoustics, and far-field spectra. Whatever frequency is captured by the shear layer is also reflected in the cavity acoustics and far-field noise radiation, indicating a frequency lock-on. This consistency suggests that the implementation of an elastic panel does not induce significant alterations in the aeroacoustic processes for these cases. However, the $EP30$ case stands out, as there is a notable disruption in the aeroacoustic coupling: the shear layer and cavity acoustics do not share the same dominant frequency. This divergence implies a breakdown in the coupling for this case, resulting in disparate dominant frequencies in the shear layer and cavity acoustic spectra.

In summary, it is determined that under certain free-stream flow conditions, specifically for $RC20$ and $RC30$, the deep cavity exhibits a robust acoustic response, with sound pressure levels reaching 86.3 dB and 87.4 dB, respectively. This is attributed to the aeroacoustic coupling between the shear layer and the cavity acoustics, where the effective impingement of the shear layer at the cavity trailing edge gives rise to pronounced cavity acoustic modes. When an elastic panel is introduced at the cavity bottom, it interacts with these cavity acoustic modes, potentially absorbing the energy of the incident acoustic waves and thereby significantly reducing the peak amplitude up to 16.1 dB, as evidenced in the $EP30$ case. By weakening the aeroacoustic coupling through the interaction between the aeroacoustic and structural dynamics—specifically the interplay of shear layer oscillations, acoustic mode resonances, and panel vibrations—the overall acoustic emissions are attenuated. Notably, the $RC10$ and $RC40$ cases do not exhibit hallmark features of aeroacoustic coupling, resulting in reduced cavity noise emissions compared to the $RC20$ and $RC30$ configurations. Consequently, the implementation of the elastic panel in the $EP10$ and $EP40$ scenarios does not yield reductions in acoustic levels as substantial as those observed in the $EP20$ and $EP30$ cases.

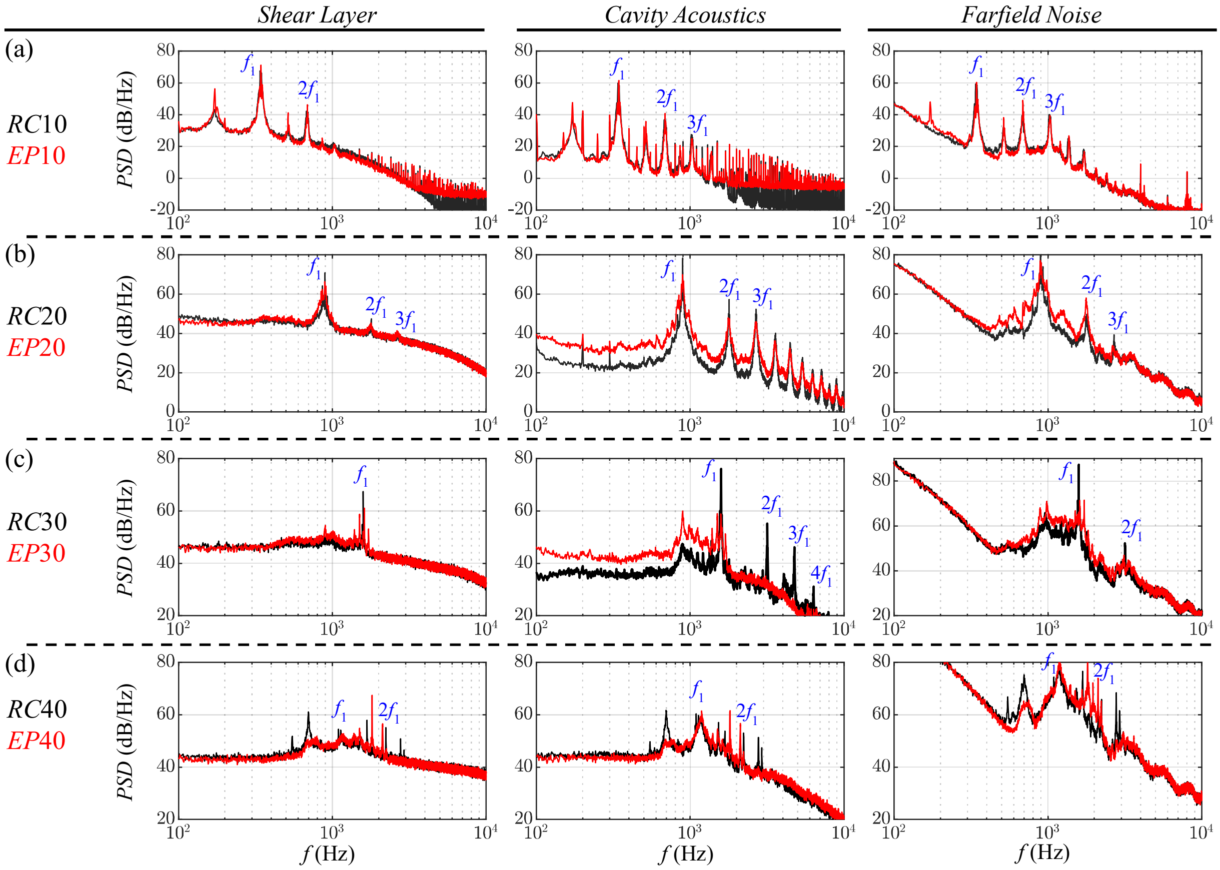

Fig. 5 Comparison of p' spectra measured at locations *mic*2 (first column), *mic*3 (second column) and *mic*1 (third column); (a) u_∞= 10 ms^{-1}, (b) u_∞= 20 ms^{-1}, (c) u_∞= 30 ms^{-1}, (d) u_∞= 40 ms^{-1}.

IV. Coherence Analysis

Our findings indicate that the pronounced acoustic response observed in *RC* configurations results from synergistic interactions between the convective shear layer and the cavity acoustic mode. This interaction is characterized by a frequency lock-on effect, which facilitates the transfer of energy from the shear layer to the cavity acoustic field. The extent of energy transfer varies with the freestream flow conditions, as some cases experience fluid resonant and some experience dynamic cavity oscillations. Therefore, the application of elastic panels yields varied levels of effectiveness in reducing the cavity noise. Some panel cases (*EP*20 and *EP*30) effectively reduce the peak spectral tones while maintaining the overall trend, whereas others (*EP*10 and *EP*40) exhibit negligible impact on the shear layer and acoustic spectra. To further investigate the factors contributing to the effectiveness of these panels, we have performed a coherence analysis on the pressure signals from the shear layer, cavity acoustic mode, and farfield noise. Figure 6 presents the coherence of these pressure signals, calculated using the formula $\gamma^2(f) = |P_{XY}(f)|^2/P_X(f)P_Y(f)$, where $P_X(f)$ and $P_Y(f)$ represent the power spectral densities of the p' signals for any selected pair among the shear layer, acoustic mode and farfield, whereas $P_{XY}(f)$ denotes the cross-power spectral density between the selected pair of signals across the shear layer, cavity acoustics and farfield noise.

For a free stream flow condition with u_∞ = 10 ms^{-1} (Figure 6(a)), both the *RC*10 and *EP*10 configurations exhibit strong coherence between the shear layer and the farfield noise at specific spectral peaks across the low-frequency region ($f < 10^3$). A similar coherence trend is also observed between the shear layer and the cavity acoustics. Additionally, the coherence between cavity acoustics and farfield noise shows strong congruence over a broad lower frequency spectrum ($10^2 < f < 10^3$). Notably, little to no difference is observed in the coherence patterns for *RC*10 and *EP*10, suggesting that the elastic panel did not significantly alter the coherence pattern of the radiating frequency modes among the components responsible for cavity noise emission, which largely remains unaffected.

As the wind speed increases to u_∞= 20 ms^{-1} (Figure 6(b)), the coherence between the shear layer and farfield noise is strengthened ($\gamma^2 \sim 0.8$) and concentrated to a solitary spectral peak at f = 895 Hz, similarly the coherence pattern of cavity-acoustics ↔ far-field noise (instead of being scattered as seen in *RC*10) remains concentrated to a solitary spectral peak at f = 895 Hz which is translated into the strongly coherent cavity acoustic mode at the same frequency mode whereas the coherence pattern between cavity acoustics and farfield noise also suggests that both of them remain strongly linked together and an overall cohesive approach which puts *RC*20 into the category of fluid resonant cavity oscillation. When the elastic panel configuration (*EP*20) is introduced under similar conditions, it slightly broadens the coherence spectrum towards the lower frequency region ($f < 10^3$) for both shear layer ↔ cavity acoustics and shear layer ↔ farfield interactions while maintaining strong coherence at f = 895Hz. However, this comes at the expense of diminished coherence at higher spectral peaks ($f > 10^3$) compared to *RC*20. Thus, it can be argued that spreading the influence of favourable coherence, instead of being concentrated at a few spectral peaks, enhances the broadband component of the signal and thus reduces the tonal noise, as observed in the corresponding *EP*20 spectra shown in Figure 5.

Overall, the cases *RC*30 and *EP*30 (Figure 6(c)) exhibited trends similar to their *RC*20 and *EP*20 counterparts. For *RC*30, there is a strong coherence between the shear layer and both farfield noise and cavity acoustics, concentrated at the peak frequency of f = 1585 Hz. In contrast, *EP*30 broadens the lower frequency coherence spectrum and reduces the strong coherency at f = 1585 Hz to $\gamma^2 \sim 0.6$, which has evidently resulted in substantial tonal noise reduction, as illustrated in Figure 5. The *RC*40 and *EP*40 cases (Figure 6(d)) generally follow a similar coherence spectrum trend as the *RC*10 and *EP*10, except the coherence is shifted towards the higher frequency region. The spectra remained scattered, and the installation of the elastic panel, while slightly reducing the coherency, did not significantly affect the ultimate noise radiation.

In essence, it is therefore suggested that fluid dynamic cavity oscillations (*RC*10 and *RC*40) are accompanied by scattered coherence spectra, leading to the emergence of various frequencies in the farfield noise spectrum (Figure 6(a) and 6(d)). Conversely, the fluid resonant cavity oscillations (*RC*20 and *RC*30) reveal coherence spectra concentrated at a few spectral peaks corresponding to the dominant flow frequencies, as observed in Figure 6(b) and 6(c). In such cases, the elastic panel is effective as it redistributes the energy of tonal frequencies and consequently reduces the tonal noise radiation associated with fluid resonant cavity oscillations.

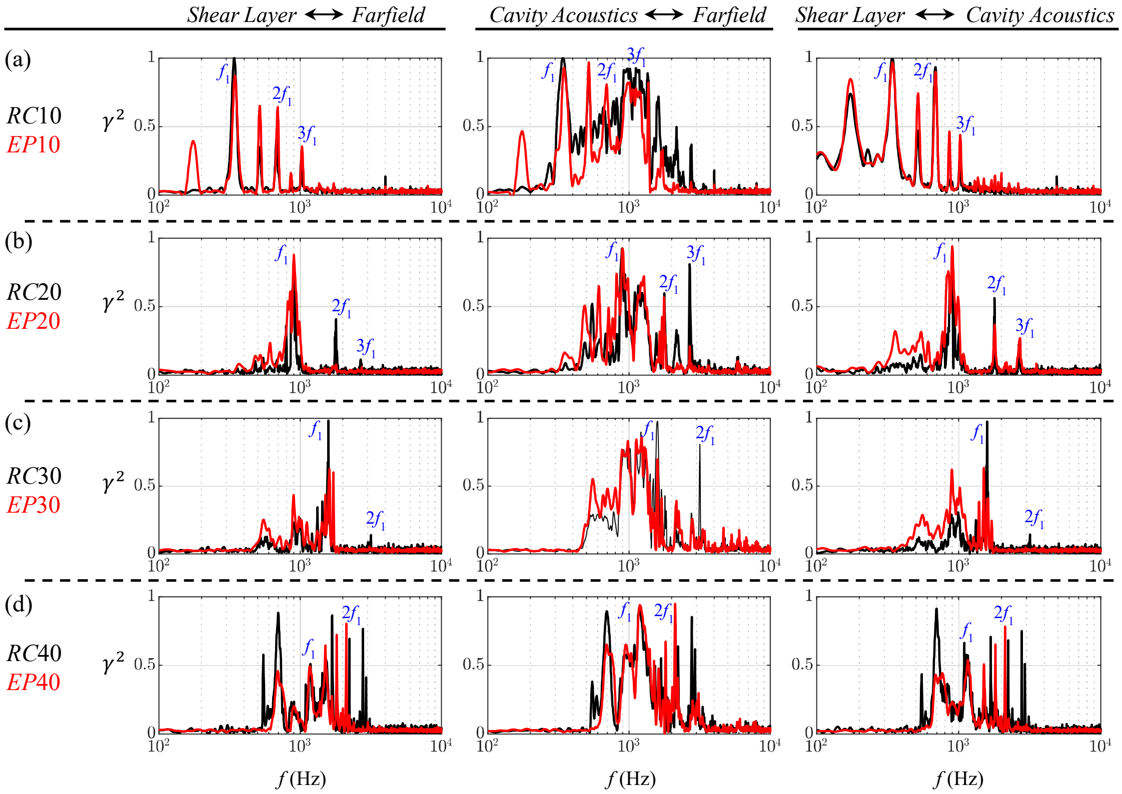

Fig. 6 Coherence, γ^2 between shear layer and farfield noise (first column), cavity acoustics and farfield noise (second column), shear layer and cavity acoustics (third column). (a) u_∞= 10 ms^{-1}, (b) u_∞= 20 ms^{-1}, (c) u_∞= 30 ms^{-1}, (d) u_∞= 40 ms^{-1}.

V. Transverse Velocity Fluctuation

The transverse velocity fields derived from PIV measurements offer crucial insights into the oscillations of the shear layer over the cavity opening, a critical site for cavity noise generation, as illustrated in Figure 7. The velocity snapshots were taken consistently at quarter-period intervals (*T*/4) within a single fluctuation cycle (*T*) of the dominant frequency. It should be noted that the period *T* varies and is specified for each tested case. The instantaneous velocity fields reveal the development of vortical structures within the shear layer, which increases in size as they are convected downstream, and their impingement on the cavity trailing edge appears as downwashes against the aft wall of the cavity. For a flow speed of u_∞= 20 ms^{-1}, the vortical structures are more distinctly defined across the cavity opening compared to those at u_∞ = 30 ms^{-1}, which are less clear. The PIV measurements suggest that flow velocities exceeding u_∞ = 30 ms^{-1} are not advisable with the current setup due to challenges in stabilizing the flow field. Typically, a flow velocity of u_∞= 20 ms^{-1} achieves optimal particle seeding density, [45], enabling accurate and reliable tracking of particles within the fluid, thus ensuring robust flow velocity data. Despite these limitations, we included the *RC*30 and *EP*30 cases to explore any potential insights.

Comparison between the *RC* and elastic panel *EP* configurations reveals subtle yet significant differences in the shear layer dynamics. In the *EP* configurations, the shear layer is slightly thinner and more disrupted compared to the well-defined vortices observed in the *RC* configurations. Moreover, the evolution of the shear layer in *EP* configurations shows notable distinctions; the onset of the shear layer at the cavity leading edge is less vigorous and robust than in *RC* configurations. Additionally, the growth pattern of the shear layer as it convects toward the cavity trailing edge differs markedly from the more regular pattern observed in *RC* cases. Lastly, the impingement of the shear layer in *EP* cases does not produce significant downwash imprints near the aft wall, unlike in *RC* cases. This observation aligns with previous findings (Figure 5) that the shear layer impingement in *EP* cases is less effective in transferring significant shear layer energy to the cavity acoustic mode compared to *RC* cases.

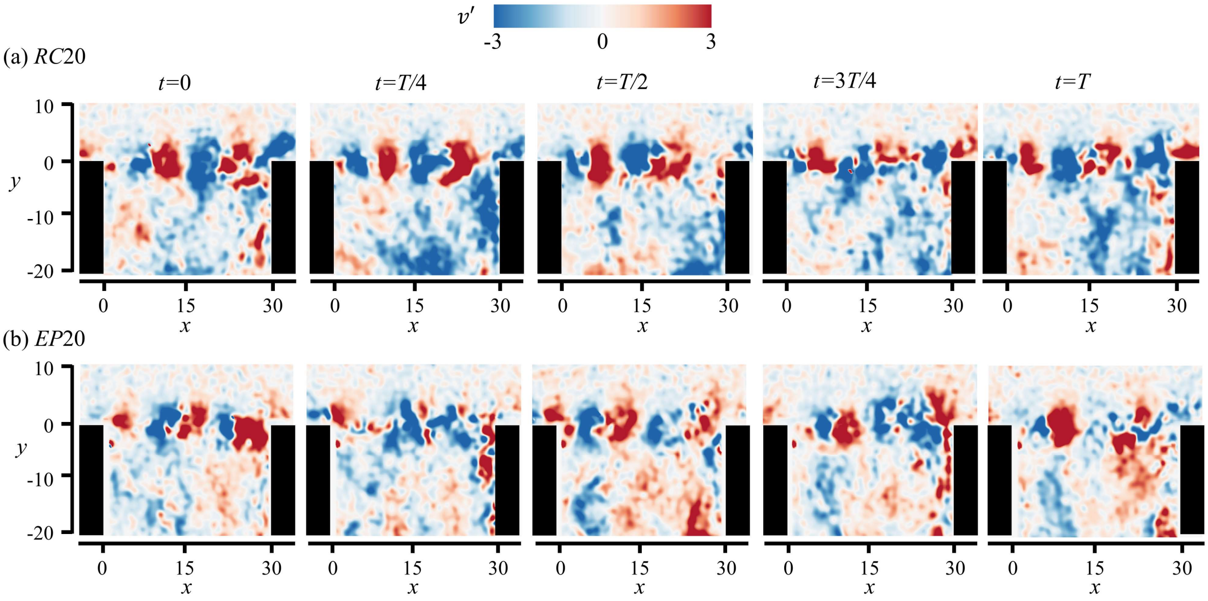

Fig. 7 Instantaneous transverse velocity fluctuation during one complete oscillation cycle of shear layer growth, followed by the downwash after impingement near the cavity opening region, (a) *RC*20, (b) *EP*20. Continued next page.

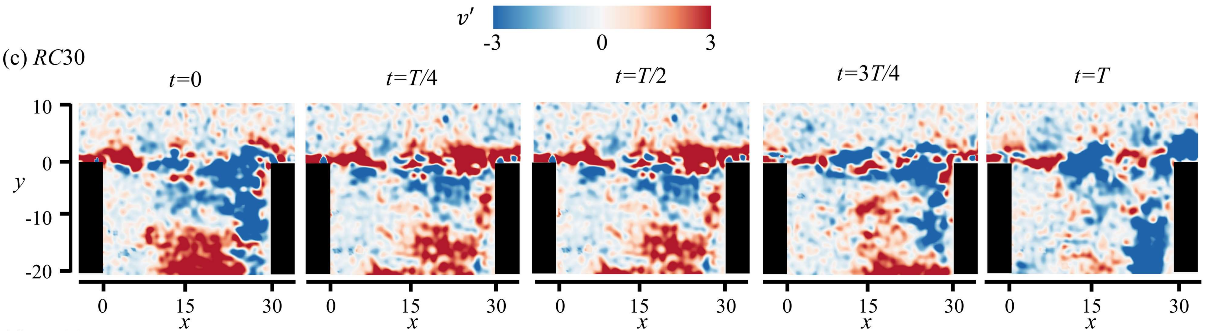
(c) *RC*30

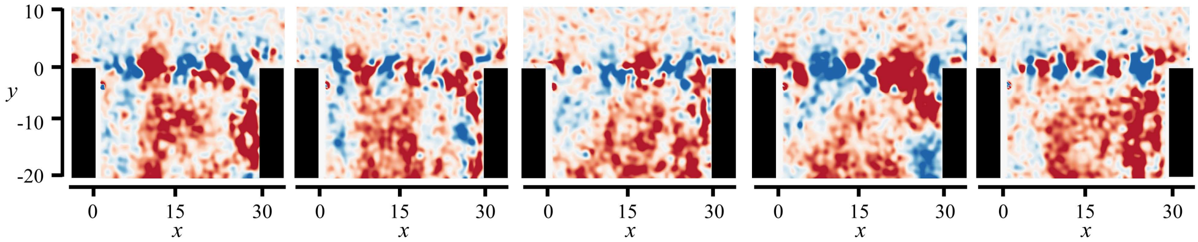
(d) *EP*30

Fig. 7 (Continues) Instantaneous transverse velocity fluctuation during one complete oscillation cycle of shear layer growth, followed by the downwash after impingement near the cavity opening region, (c) *RC*30, (d) *EP*30.

VI. Conclusion

The present experimental study aimed to corroborate and enhance the efficacy of a novel passive control method using surface compliance, previously explored numerically [1], to suppress tonal noise in deep cavities—a prevalent issue in various aeroacoustic applications. By implementing an elastic panel flush-mounted at the cavity bottom, the study sought to confirm the potential benefits of modifying aeroacoustic-structural interactions, thereby aiming to reduce acoustic emissions at critical flow velocities. This approach was designed to test the elastic panel ability to dissipate energy via vibrations, disrupting the internal aeroacoustic processes and potentially leading to significant reductions in noise output. The experimental setup in an aeroacoustic wind tunnel allowed for precise measurements of near and far-field pressures alongside a PIV setup to capture the flow dynamics. The findings revealed that the introduction of the compliant panel significantly altered the aeroacoustic patterns within the cavity, leading to notable reductions in tonal noise by 16.1 dB, particularly at flow velocities of 20 and 30 ms^{-1}. These speeds correspond to conditions where the interaction between shear layer oscillations and cavity acoustic modes typically amplifies aeroacoustic resonances in *RC* cases. Comparison between the *RC* configuration and the *EP* setup indicated that the introduction of the panel significantly affected the coherence among cavity acoustic mode ↔ shear layer ↔ farfield noise, specifically at the dominant frequency, which reduced the peak noise levels ultimately. This suggests a disruption in the typical aeroacoustic coupling processes, potentially due to the altered dynamics of the shear layer and its interaction with the cavity acoustic mode. PIV images also provided insights into the dynamics of the shear layer over the cavity opening. Notably, the elastic panel *EP* configurations demonstrated a relatively thinner and disrupted shear layer compared to the *RC* setups, where the shear layer vortices tend to be well-defined and larger as they convect downstream. Moreover, in the case of *RC* the vigorous shear layer impingement process at the cavity trailing edge indicates an effective energy transfer from the shear layer to the cavity acoustic mode, while the same could not be realized in *EP* cases which essentially differentiates and comprehend the noise generation and reduction processes in respective *RC* and *EP* cases.

Acknowledgement

The authors gratefully acknowledge the support from the Research Grants Council of the Government of Hong Kong Special Administrative Region under Grant No. 15208520. The first author is also thankful for the stipend support for his study, as well as the support provided through the Out-going Research Student Attachment Programme to SUSTech by the Department of Mechanical Engineering at The Hong Kong Polytechnic University.

References

[1] Naseer, M. R., Arif, I., Leung, R. C. K., and Lam, G. C. Y., "Suppression of deep cavity aeroacoustics at low Mach number by localized surface compliance," *Physics of Fluids,* vol. 35, no. 5, 2023.

[2] Cattafesta III, L. N., Song, Q., Williams, D. R., Rowley, C. W., and Alvi, F. S., "Active control of flow-induced cavity oscillations," *Progress in Aerospace Sciences,* vol. 44, no. 7-8, pp. 479-502, 2008.

[3] Liu, Y., Chen, B., Shi, Y., and Rong, A., "Visualization of pressure fluctuation characteristics of weapon bay on unmanned aerial vehicle using delayed detached eddy simulation," *Journal of Visualization,* vol. 27, no. 1, pp. 75-87, 2024.

[4] Talotte, C., "Aerodynamic noise: A critical survey," *Journal of Sound and Vibration,* vol. 231, no. 3, pp. 549-562, 2000.

[5] He, Y., Thompson, D., and Hu, Z., "Aerodynamic noise from a high-speed train bogie with complex geometry under a leading car," *Journal of Wind Engineering and Industrial Aerodynamics,* vol. 244, p. 105617, 2024.

[6] Kook, H. and Mongeau, L., "Analysis of the periodic pressure fluctuations induced by flow over a cavity," *Journal of Sound and Vibration,* vol. 251, no. 5, pp. 823-846, 2002.

[7] Bruggeman, J. C., Hirschberg, A., van Dongen, M. E. H., Wijnands, A. P. J., and Gorter, J., "Flow Induced Pulsations in Gas Transport Systems: Analysis of the Influence of Closed Side Branches," *Journal of Fluids Engineering,* vol. 111, no. 4, pp. 484-491, 1989.

[8] Wang, P., Jia, S., He, Z., He, C., Sung, H. J., and Liu, Y., "Flow–acoustic resonance mechanism in tandem deep cavities coupled with acoustic eigenmodes in turbulent shear layers," *Journal of Fluid Mechanics,* vol. 984, p. A19, 2024.

[9] Ziada, S. and Bühlmann, E. T., "Self-excited resonances of two side-branches in close proximity," *Journal of Fluids and Structures,* vol. 6, no. 5, pp. 583-601, 1992.

[10] Rebholz, P. S., Krebietke, S., Abhari, R. S., and Kalfas, A. I., "Turbine Aerodynamic Low-Frequency Oscillation and Noise Reduction Using Partial Shrouds," *Journal of Propulsion and Power,* vol. 32, no. 5, pp. 1067-1076, 2016.

[11] Ziada, S., Oengören, A., and Vogel, A., "Acoustic resonance in the inlet scroll of a turbo-compressor," *Journal of Fluids and Structures,* vol. 16, no. 3, pp. 361-373, 2002.

[12] Covert, E. E., "An approximate calculation of the onset velocity of cavity oscillations," *AIAA Journal,* vol. 8, no. 12, pp. 2189-2194, 1970.

[13] Heller, H. H. and Bliss, D. B., "Aerodynamically induced pressure oscillations in cavities - physical mechanisms and suppression concepts," *AF Flight Dynamics Laboratory, (FY), Wright-Patterson AFB, Ohio,* pp. Technical Report No. AFFDL-TR-74-133, 1975.

[14] Rockwell, D. and Naudascher, E., "Review—Self-sustaining oscillations of flow past cavities," *Journal of Fluids Engineering,* vol. 100, no. 2, pp. 152-165, 1978.

[15] Rossiter, J. E., "Wind-tunnel experiments on the flow over rectangular cavities at subsonic and transonic speeds," *Aeronautical Research Council,* p. Reports and Memoranda No. 3438, 1964.

[16] Arya, N. and De, A., "Effect of vortex and entropy sources in sound generation for compressible cavity flow," *Physics of Fluids,* vol. 33, no. 4, p. 046107, 2021.

[17] Liu, Q. and Gaitonde, D., "Acoustic response of turbulent cavity flow using resolvent analysis," *Physics of Fluids,* vol. 33, no. 5, p. 056102, 2021.

[18] East, L. F., "Aerodynamically induced resonance in rectangular cavities," *Journal of Sound Vibration,* vol. 3, no. 3, pp. 277-287, 1966.

[19] Ho, Y. W. and Kim, J. W., "A wall-resolved large-eddy simulation of deep cavity flow in acoustic resonance," *Journal of Fluid Mechanics,* vol. 917, 2021.

[20] Howe, M. S., "Vortex sound," in *Theory of Vortex Sound*, (Cambridge Texts in Applied Mathematics. Cambridge: Cambridge University Press, 2002, pp. 114-135.

[21] Yang, Y., Rockwell, D., Lai-Fook Cody, K., and Pollack, M., "Generation of tones due to flow past a deep cavity: Effect of streamwise length," *Journal of Fluids and Structures,* vol. 25, no. 2, pp. 364-388, 2009.

[22] Yokoyama, H., Odawara, H., and Iida, A., "Effects of freestream turbulence on cavity tone and sound source," *International Journal of Aerospace Engineering,* vol. 2016, p. 7347106, 2016.

[23] Abdelmwgoud, M. and Mohany, A., "Control of the self-sustained shear layer oscillations over rectangular cavities using high-frequency vortex generators," *Physics of Fluids,* vol. 33, no. 4, p. 045115, 2021.

[24] Lee, B., "Effect of a Perturbed Shear Layer on Cavity Resonance," *Journal of Aircraft,* vol. 47, no. 1, pp. 343-345, 2010.

[25] Li, B., Ye, C.-C., Wan, Z.-H., Liu, N.-S., Sun, D.-J., and Lu, X.-Y., "Noise control of subsonic flow past open cavities based on porous floors," *Physics of Fluids,* vol. 32, no. 12, p. 125101, 2020.

[26] Liu, Q. and Gómez, F., "Role of trailing-edge geometry in open cavity flow control," *AIAA Journal,* vol. 57, no. 2, pp. 876-878, 2019.

[27] Mourão Bento, H. F., VanDercreek, C. P., Avallone, F., Ragni, D., and Snellen, M., "Lattice Boltzmann very large eddy simulations of a turbulent flow over covered and uncovered cavities," *Physics of Fluids,* vol. 34, no. 10, p. 105120, 2022.

[28] Maury, C., Bravo, T., and Mazzoni, D., "The use of microperforations to attenuate the cavity pressure fluctuations induced by a low-speed flow," *Journal of Sound and Vibration,* vol. 439, pp. 1-16, 2019.

[29] Yokoyama, H., Otsuka, K., Otake, K., Nishikawara, M., and Yanada, H., "Control of cavity flow with acoustic radiation by an intermittently driven plasma actuator," *Physics of Fluids,* vol. 32, no. 10, p. 106104, 2020.

[30] Bacci, D. and Saddington, A. J., "Influence of door gap on aeroacoustics and structural response of a cavity," *AIAA Journal,* vol. 62, no. 3, pp. 1021-1036, 2023.

[31] Bacci, D. and Saddington, A. J., "Hilbert–Huang spectral analysis of cavity flows incorporating fluidic spoilers," *AIAA Journal,* vol. 61, no. 1, pp. 271-284, 2022.

[32] Saddington, A. J., Thangamani, V., and Knowles, K., "Comparison of passive flow control methods for a cavity in transonic flow," *Journal of Aircraft,* vol. 53, no. 5, pp. 1439-1447, 2016.

[33] Yang, Y. *et al.*, "Design, validation, and benchmark tests of the aeroacoustic wind tunnel in SUSTech," *Applied Acoustics,* vol. 175, p. 107847, 2021.

[34] Angland, D., Zhang, X., and Goodyer, M., "Use of Blowing Flow Control to Reduce Bluff Body Interaction Noise," *AIAA Journal,* vol. 50, no. 8, pp. 1670-1684, 2012.

[35] Vemuri, S. S., Liu, X., Zang, B., and Azarpeyvand, M., "On the use of leading-edge serrations for noise control in a tandem airfoil configuration," *Physics of Fluids,* vol. 32, no. 7, p. 077102, 2020.

[36] Maryami, R. and Liu, Y., "Cylinder flow and noise control by active base blowing," *Journal of Fluid Mechanics,* vol. 985, p. A10, 2024.

[37] Narasimha, R. and Prasad, S. N., "Leading edge shape for flat plate boundary layer studies," *Experiments in Fluids,* vol. 17, no. 5, pp. 358-360, 1994.

[38] Moreau, D. J., Brooks, L. A., and Doolan, C. J., "The effect of boundary layer type on trailing edge noise from sharp-edged flat plates at low-to-moderate Reynolds number," *Journal of Sound and Vibration,* vol. 331, no. 17, pp. 3976-3988, 2012.

[39] Naseer, M. R., Arif, I., Lam, G. C. Y., and Leung, R. C. K., "Effect of Flow-Induced Surface Vibration on Deep Cavity Aeroacoustics," *AIAA Paper No,* pp. 2022-2958, 2022.

[40] Yokoyama, H., Tanimoto, I., and Iida, A., "Experimental tests and aeroacoustic simulations of the control of cavity tone by plasma actuators," *Applied Sciences,* vol. 7, no. 8, p. 790, 2017.

[41] Elder, S. A., "Self-excited depth-mode resonance for a wall-mounted cavity in turbulent flow," *Journal of the Acoustical Society of America,* vol. 64, no. 3, pp. 877-890, 1978.

[42] Forestier, N., Jacquin, L., and Geffroy, P., "The mixing layer over a deep cavity at high-subsonic speed," *Journal of Fluid Mechanics,* vol. 475, pp. 101-145, 2003.

[43] Samimy, M. *et al.*, "Feedback control of subsonic cavity flows using reduced-order models," *Journal of Fluid Mechanics,* vol. 579, pp. 315-346, 2007.

[44] Naseer, M. R., Arif, I., and Leung, R. C. K., "Utilization of Embedded Surface Compliance for Suppression of Deep Cavity Flow Noise," *INTER-NOISE and NOISE-CON Congress and Conference Proceedings,* vol. 268, no. 3, pp. 5323-5334, 2023.

[45] Maryami, R., Arcondoulis, E. J. G., and Liu, Y., "Flow and aerodynamic noise control of a circular cylinder by local blowing," *Journal of Fluid Mechanics,* vol. 980, p. A56, 2024.